Robotic Adherent Cell Injection for Characterizing Cell–Cell Communication

Jun Liu, *Student Member, IEEE*, Vinayakumar Siragam, Zheng Gong, *Member, IEEE*, Jun Chen, Michael D. Fridman, Clement Leung, *Member, IEEE*, Zhe Lu, *Member, IEEE*, Changhai Ru, Shaorong Xie, Jun Luo, Robert M. Hamilton, and Yu Sun*, *Senior Member, IEEE*

***Abstract*—Compared to robotic injection of suspended cells (e.g., embryos and oocytes), fewer attempts were made to automate the injection of adherent cells (e.g., cancer cells and cardiomyocytes) due to their smaller size, highly irregular morphology, small thickness (a few micrometers thick), and large variations in thickness across cells. This paper presents a robotic system for automated microinjection of adherent cells. The system is embedded with several new capabilities: automatically locating micropipette tips; robustly detecting the contact of micropipette tip with cell culturing surface and directly with cell membrane; and precisely compensating for accumulative positioning errors. These new capabilities make it practical to perform adherent cell microinjection truly via computer mouse clicking in front of a computer monitor, on hundreds and thousands of cells per experiment (versus a few to tens of cells as state of the art). System operation speed, success rate, and cell viability rate were quantitatively evaluated based on robotic microinjection of over 4000 cells. This paper also reports the use of the new robotic system to perform cell–cell communication studies using large sample sizes. The gap junction function in a cardiac muscle cell line (HL-1 cells), for the first time, was quantified with the system.**

***Index Terms*—Cell communication, drug testing, gap junction, microinjection, robotics, toxicology testing.**

I. Introduction

INTERCELLULAR communication is a critical part of cellular activities and coordinates cell functions [1]. Disorders of intercellular communication are responsible for diseases such as cancer [2], autoimmunity [3], and diabetes [4]. A standard technique for measuring intercellular communication is based on monitoring transfer of fluorescent molecules from an individual cell to adjacent cells through functional gap junctions (see Fig. 1). The quantitative measurement of dye transfer requires injection of fluorescent molecules into single cells. In present gap junction testing experiments, only a few or tens of cells can be injected due to the limitations of manual operation, posing a practical hurdle in attaining statistically significant data, for instance, for testing drug molecules on the alteration of gap junction function [5].

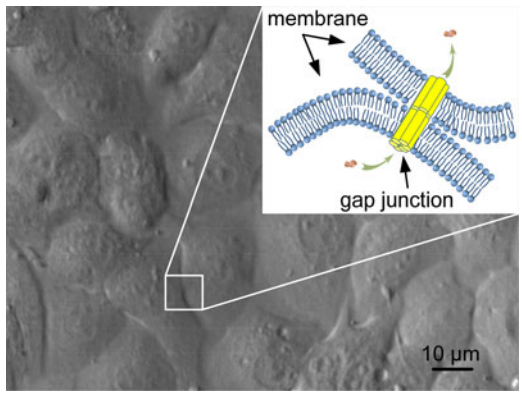

Fig. 1. Adherent cells (HL-1) under 20×. Inset shows the schematic of a gap junction for cell–cell communication.

Manually manipulating single cells is tedious and time consuming and has high skill requirements. In manual operation, a skilled operator must dexterously control multiple devices such as micromanipulator, pump, and microscope stage. Robotic cell manipulation technologies progressed significantly over the past decade. The vast majority of demonstrated robotic systems focused on the manipulation of suspended cells (i.e., oocytes and embryos) [6]–[11]. Fewer attempts were made to automate the injection of adherent cells.

Most mammalian cells (e.g., cancer cells and cardiomyocytes) adhere to a culturing surface. Different from large suspend cells (e.g., mouse oocytes∼100 μm; zebrafish embryos∼1 mm), adherent cells are smaller in size and highly irregular in morphology (versus spherical for oocytes/embryos), making robust pattern recognition difficult and automation challenging [12]. Additionally, adherent cells are only a few micrometers thick and vary significantly in thickness, posing more stringent requirements in robotic positioning.

Manuscript received May 22, 2014; revised July 14, 2014; accepted July 20, 2014. Date of publication July 24, 2014; date of current version December 18, 2014. This work was supported by the Natural Sciences and Engineering Research Council of Canada, Ontario Centres of Excellence, the Canadian Institutes of Health Research, and Shanghai Municipal Science and Technology Commission Project under Grant 14JC1491500. *Asterisk indicates corresponding author.*

J. Liu, Z. Gong, J. Chen, C. Leung, and Z. Lu are with the Department of Mechanical and Industrial Engineering, University of Toronto, Toronto, ON M5S 3G8, Canada (e-mail: ljun@mie.utoronto.ca; zgong@mie.utoronto.ca; junchen@mie.utoronto.ca; clement.leung@utoronto.ca; zhe.lu@utoronto.ca).

V. Siragam, M. D. Fridman, and R. M. Hamilton are with the Division of Cardiology, The Hospital for Sick Children, Toronto, ON M5G 1X8, Canada (e-mail: vsiragam@gmail.com; michaeldfridman@gmail.com; robert.hamilton@sickkids.ca).

*Y. Sun is with the Department of Mechanical and Industrial Engineering, University of Toronto, Toronto, ON M5S 3G8, Canada, the College of Automation, Harbin Engineering University, Harbin 150001, China, and also with the School of Mechatronic Engineering and Automation, Shanghai University, Shanghai 200072, China (e-mail: sun@mie.utoronto.ca).

C. Ru is with the College of Automation, Harbin Engineering University, Harbin 150001, China (e-mail: rchhai@gmail.com).

S. Xie and J. Luo are with the School of Mechatronic Engineering and Automation, Shanghai University, Shanghai 200072, China (e-mail: srxie@shu.edu.cn; luojun@shu.edu.cn).

Color versions of one or more of the figures in this paper are available online at http://ieeexplore.ieee.org.

Digital Object Identifier 10.1109/TBME.2014.2342036

A few joystick-based systems were demonstrated to assist operators for adherent cell microinjection [13], [14]. Long training, low success rates, and poor reproducibility make these systems incapable of injecting more than tens of cells per experiment. For example, the most popular commercial system for adherent cell injection is Eppendorf's InjectMan system that requires an operator to look into the eyepieces of a microscope and perform microinjection by controlling joysticks. The injection success rate and cell survival rate of the system are 49.2% and 49.72%, respectively [13]. The only other joystick-based adherent cell injection system was demonstrated for the injection of fluorescent molecules into adherent cell lines with a 49% injection success rate [14]. Due to the difficulty of operating joysticks for fine positioning control, this system does not permit the injection of a high number of cells (only 82 cells injected). An automated system integrating a cell detection algorithm reported in [15] produced a success rate of 67% at a speed of 7–8 cells/min.

In our previous study in robotic injection of adherent cells [16], we attempted to transform joystick-based operation to computer mouse clicking. However, several practical limitations in the system required the operator to manually perform a few key steps using joysticks and look into the eyepieces of the microscope. This hybrid way of system operation (mouse clicking in front of a computer monitor and operating joysticks under microscope) precluded the system's potential for routine use in biology labs. First, the system lacked the critical capability for automatically locating a micropipette tip. In adherent cell injection, the size of micropipette tip must be kept within a few hundreds of nanometers to ensure a high cell viability. Locating the tip under optical microscopy requires high skills and extreme care since tip breakage can easily occur. Additionally, the small tip often gets clogged by large molecules or cell debris, necessitating regular replacement of micropipette tips (e.g., every 100 cells), demanding the system to possess the capability for locating micropipette tip automatically.

The second limitation in our previous system was the limited contact detection capability. In experiments, adherent cells are often cultured on gels or protein-coated (e.g., collagen) surfaces. Our previously reported contact detection algorithm works well on a bare culturing surface but has a low success rate on these coated surfaces. Furthermore, the previous contact detection algorithm is not applicable when cell confluency (i.e., density) is high (>80%). Third, the previous system was not able to compensate for accumulated positioning errors, which made the system unable to inject more than 100 cells.

In this study, we present a new robotic system capable of injecting thousands of adherent cells. The system successfully addresses the limitations of our previous system prototype [16] and has the following new capabilities: automatically locating micropipette tips; robustly detecting the contact of micropipette tip with cell culturing surface and directly with cell membrane; and precisely compensating for accumulative positioning errors. These new capabilities, for the first time, make it practical to perform adherent cell microinjection truly via computer mouse clicking in front of a computer monitor, making the robotic system suitable for routine use in biology labs. We also demonstrate the use of the new robotic system to perform cell–cell communication studies with large sample sizes (over 1000 cells versus a few to tens of cells as state of the art). Finally, the gap junction function in a cardiac muscle cell line (HL-1 cells), for the first time, was quantified with the new robotic system.

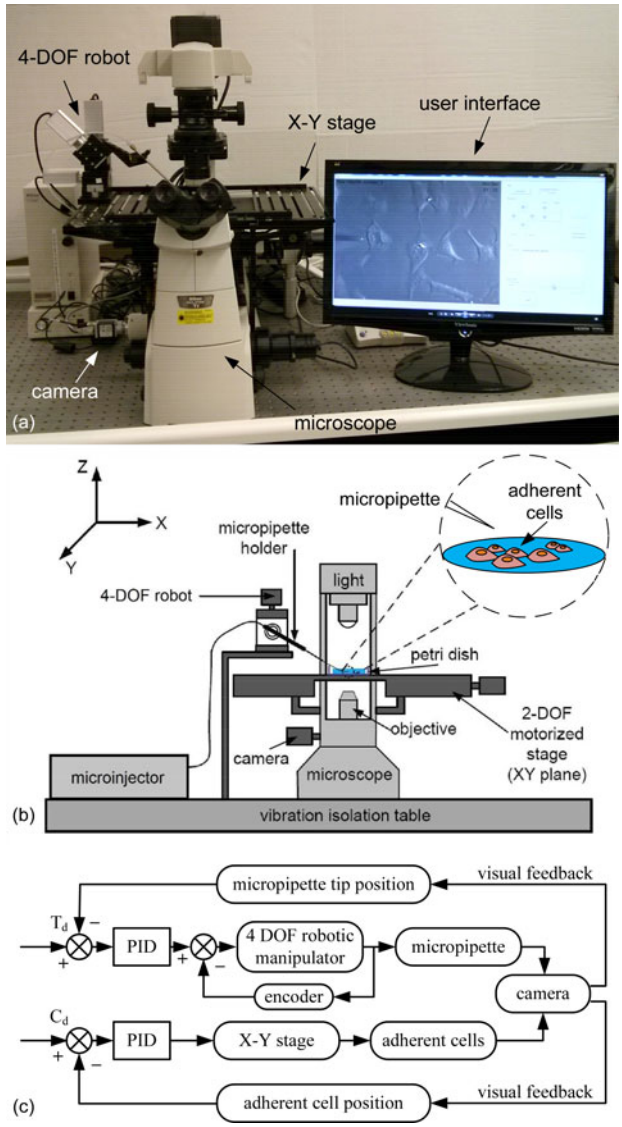

Fig. 2. (a) and (b) RACI system. (c) System control architecture.

II. System Overview

This system uses well-calibrated air pressure to deliver aqueous solution into either the cytoplasm or nucleus of a cell. As shown in Fig. 2(a) and (b), the system consists of a standard inverted microscope (Nikon TE2000-S, Nikon Microscopes) and a motorized *X–Y* translational stage (ProScan, Prior Scientific, Inc.). The *X–Y* stage has a travel range of 75 mm along both axes with a resolution of 0.01 μm, the maximum speed of 5 mm/s, and a repeatability of ± 1 μm. A CMOS camera (acA1300-32 gm, Basler) is connected to the microscope for visual feedback. A glass micropipette, laser pulled to have an outer diameter of 500 nm and an inner diameter of 300 nm, is mounted to a 4-DOF micromanipulator (MX7600, Siskiyou, Inc.) that has a travel range of 20 mm and a 0.1-μm positioning resolution along each axis. A host computer executing

computer vision microscopy and motion control algorithms controls all hardware.

The robotic micromanipulator and *X–Y* stage are cooperatively controlled for positioning the micropipette along the *XYZ* axes and positioning cells in the *XY* plane, respectively. The overall control architecture of the system is summarized in Fig. 2(c). Microscopy visual feedback is used to control the positioning of the micromanipulator and *X–Y* stage, forming an image-based visual servo control system.

When a micropipette is mounted on the system, the system detects the micropipette tip's position and automatically moves it to the center of the field of view (see Section III-A). The system is capable of detecting the contact in two modes, either on cell culturing surface or directly on cell membrane (see Sections III-B and III-C), to determine the relative vertical distance between the micropipette tip and the cells in the *Z* direction. After the injection location (inside cytoplasm or nucleus) on each cell is selected via computer mouse clicking, the system controls the micropipette to deliver a precise volume into each cell, and completes the injection of all selected cells following the shortest path. The system then controls the *X–Y* translational stage to bring cells in the next field of view under microscopy imaging for injection.

III. Key Methods

A. Locating Micropipette Tip

When a micropipette tip is mounted on the micromanipulator, the system automatically locates the micropipette tip and moves it to the center of the field of view. This process involves two main steps: micropipette detection and autofocus adjustment.

In the detection step, the micropipette is swept in the *XY* plane for detecting its presence in the field of view. In some cases, the micropipette tip cannot be detected when it is far away from the focal plane. When this occurs, the system moves the focal plane up by controlling the focus adjustment motor, and the *X–Y* sweep is then repeated. During the sweep of the micropipette, motion history images (MHI) are generated and used for detecting the presence of the micropipette. The MHI method is discussed in Section III-C.

In the autofocus step, the system uses the normalized variance method [17] to calculate the focus measure. The autofocus step consists of coarse and fine focus adjustments. Coarse focus adjustment moves the focal plane in a large step size until the entire image produces a maximal focus measure value. In fine focus adjustment, a recursive quad-tree autofocusing method is used to accurately focus on the micropipette tip with smaller step sizes. After the focus adjustments, the in-focus micropipette tip is moved to the center of the field of view through closed-loop visual servoing under a low magnification objective and then under a high magnification objective. The detailed methods for detecting and tracking micropipette tips are described in [18].

B. Contact Detection on Cell Culture Surface

In order to inject materials into a cell, the relative vertical distance between the micropipette tip and the cell along the *Z*-direction must be accurately detected. Without the inclusion of an extra sensor (e.g., tactile or force sensors), which increases hardware complexity [19], two modes of computer vision-based contact detection algorithms are developed to accurately determine the relative heights of the micropipette tip and adherent cells. This section describes the first mode, in which the system detects the initial contact of micropipette tip on the cell culturing surface that is protein coated (versus bare surface).

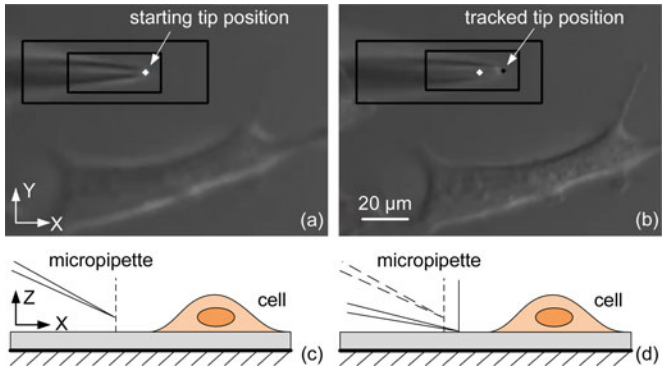

Fig. 3. Detection of contact on cell culture surface. (a) Micropipette tip is lowered toward the cell culture surface while the *X–Y* stage moves along the *X* axis from left to right. (b) Micropipette tip slides horizontally when it contacts the culture surface. (c) and (d) Schematic side view of (a) and (b).

1) Empty Region Detection: When cell confluency is lower than 80%, empty areas on the culturing surface can be detected and used for contact detection. The system divides the field of view into subregions, the size of which is 100 pixels$\times$100 pixels. The normalized variance of the pixel value, F, is calculated for each region to represent its smoothness, according to

$$F = \frac{1}{W \cdot H \cdot \mu} \sum_{W} \sum_{H} (I(x,y) - \mu)^2 \tag{1}$$

where W and H are the region width and height, $I(x,y)$ is the pixel intensity at the point (x,y), and μ is the average region intensity. This algorithm effectively compensates for differences in average intensity among different regions. The region with the lowest variance value is considered empty and used for performing contact detection.

2) Contact Detection via Three-Dimensional Motion: The system moves the detected empty region in the *XY* plane until it is directly under the micropipette tip [see Fig. 3(a) and (c)]. The micropipette tip is then lowered by the micromanipulator along the *Z* direction. When the micropipette tip contacts the bare surface of a Petri dish, further vertical movement of the micropipette tip induces horizontal motion [20]. However, in cell culturing, the Petri dish surface is usually coated with gel or protein (e.g., collagen). The coating makes it difficult for the micropipette tip to "slide" horizontally (it "stabs" directly into the coated layer). Therefore, in this system, the *X–Y* stage is also servoed simultaneously to move along the direction in which micropipette tip enters the field of view, while the micropipette tip is being lowered by the micromanipulator. The *X–Y* stage's motion enables the reliable generation of the pipette tip's horizontal "sliding" motion [see Fig. 3(b) and (d)], resulting in highly reliable contact detection on protein-coated cell culture surfaces.

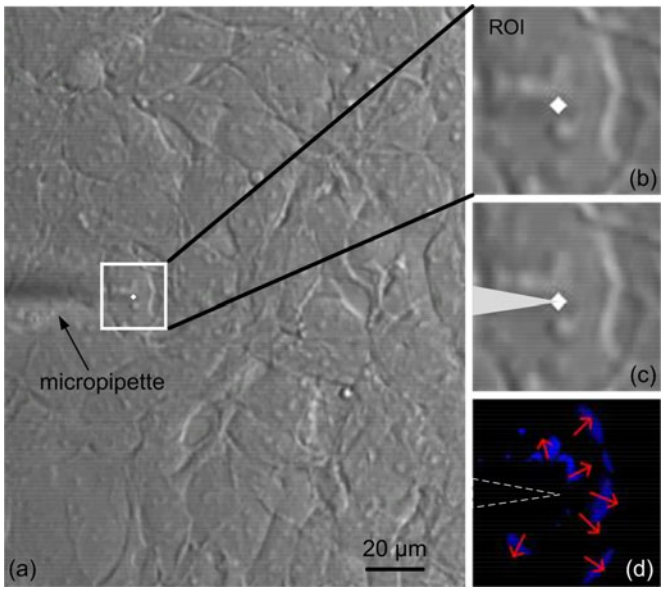

Fig. 4. Detection of contact on cell surface. (a) At high cell confluency, the system detects direct contact of the pipette tip on the cell surface. (b) ROI image shows cell being deformed: white dot indicates tip position. (c) Modified ROI removing the motion of micropipette tip. (d) MHI showing the deformation of cell: red arrows indicate motion gradients.

C. Contact Detection on Cell Membrane

When cell confluency is high, empty regions on the culture surface become unavailable; hence, the system performs contact detection by detecting direct contact of the micropipette tip on the cell membrane [see Fig. 4(a)]. After the operator selects a cell via computer mouse clicking, the system moves the cell to the micropipette tip position in *XY* plane and then moves the micropipette tip downwards along the *Z* axis. When the micropipette tip contacts the cell membrane, the cell is deformed and a subtle motion appears around the contact point. To detect this subtle motion, we developed an algorithm based on MHI. The MHI-based method enhances motion representation by accumulating cell deformation over a period of time.

A region of interest (ROI) is first obtained around the micropipette tip [see Fig. 4(b)]. Within the ROI, the image is

$$I(x,y,t) = b_t(x,y) + m_t(x,y) + n_t(x,y) \tag{2}$$

where $b_t(x,y)$ is the static background; $m_t(x,y)$ is the moving object; $n_t(x,y)$ is the background noise; and t is time. The moving object is extracted via taking the difference between consecutive frames.

$$\begin{aligned} D(x,y,t) &= I(x,y,t+1) - I(x,y,t) \\ &= M(x,y,t) + N(x,y,t) \end{aligned} \tag{3}$$

where $M(x,y,t)$ is the motion region; $N(x,y,t)$ is noise; and $D(x,y,t)$ is the difference image containing the moving object and background aberration due to motion and noise. Background aberration can lead to incorrect detection (e.g., motion ambiguity and distortion) and make detection fail when object motion speed is low.

In our system, the motion region $M(x,y,t)$ contains motion from both the lowering micropipette and cell deformation due to micropipette–cell contact. Hence

$$M(x,y,t) = M_p(x,y,t) + M_c(x,y,t) \tag{4}$$

where $M_p(x,y,t)$ is the micropipette lowering motion and $M_c(x,y,t)$ is the motion from cell deformation. When the micropipette is moved along *Z* axis during contact detection, the tip's location in the *XY* plane, (x_p, y_p), is constant, and the lowering motion results from the defocusing phenomenon. Since a defocusing blurred image is equivalent to an exponential decay function [21], the micropipette lowering motion can be described as $M_p(x,y,t) = M(x_p,y_p,t_0) * e^{-\lambda t}$, where $M(x_p,y_p,t_0)$ is the initial micropipette's motion before cell contact occurs. Thus, motion from cell deformation is

$$M_c(x,y,t) = M(x,y,t) - M(x_p,y_p,t_0) * e^{-\lambda t}. \tag{5}$$

Since the micropipette is controlled to move downwards at a constant speed v, its *Z*-displacement is proportional to time t. Hence, the cell deformation term can also be expressed as a function of *Z*-displacement, $M_c(x,y,t) = M_c(x,y,Z/v)$. After removing micropipette tip's motion, the noise term $N(x,y,t)$ in the difference image can be removed by a Gaussian low-pass filter and image binarization. The binary image representing cell deformation-caused motion is

$$\Psi(x,y,t) = \begin{cases} 1, & \text{if } \mathrm{M_c}(x,y,t) > \xi \\ 0, & \text{otherwise.} \end{cases} \tag{6}$$

The MHI is

$$H_\tau(x,y,t) = \begin{cases} \tau, & \text{if } \Psi(x,y,t) = 1 \\ \max(0,\ H_\tau(x,y,t-1) - \gamma), & \text{otherwise} \end{cases} \tag{7}$$

where the duration τ determines the temporal extent of the movement and γ is the decay parameter. The subtle cell deforming motion is greatly enhanced by adding the motion history information [see Fig. 4(d)].

The sum of pixel values in MHI, $s(H)$, is calculated as a measure to determine the contact of cell membrane. If $s(H)$ is above a threshold value δ, the micropipette tip is considered as contacting cell top membrane. The threshold δ is calculated dynamically by analyzing MHIs in which the micropipette tip has not contacted cell surface.

$$\delta = \bar{s} + a \cdot \sigma(s) \tag{8}$$

where $\bar{s}$ is the average of MHIs' sum of pixel values before cell contact occurs; $\sigma(s)$ is the standard deviation; and a is a preset parameter which is experimentally determined. By adding $a \cdot \sigma(s)$ to the mean value, the threshold δ effectively rejects those MHIs that do not contain cell deformation. In addition, the motion gradient of the MHI is also used to avoid false positive detection. The motion gradient is computed by convolution with Sobel filters to yield spatial derivatives, $F_x(x,y)$ and $F_y(x,y)$.

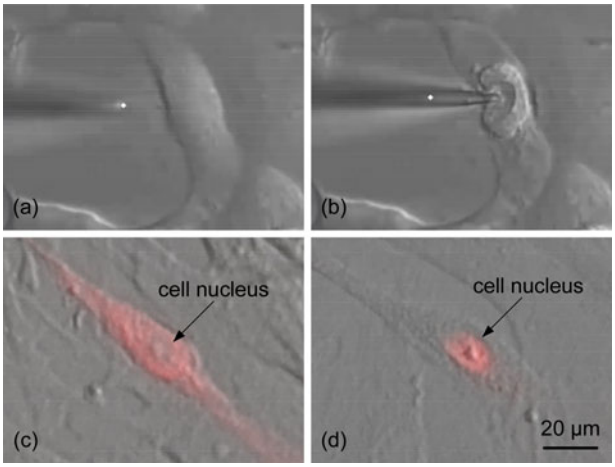

Fig. 5. Robotic injection of adherent cells. (a) and (b) When the micropipette is inserted into the cell, material deposition triggered by pressure pulses results in a "shock wave" motion inside the cell. (c) Fluorescence is present only in cytoplasm. (d) Fluorescence is present only in cell nucleus.

The orientation of the motion gradient at each pixel is

$$\Phi(x,y) = \arctan \frac{F_y(x,y)}{F_x(x,y)}. \tag{9}$$

As the micropipette tip touches the cell membrane, deformation occurs around the contact point. Accordingly, the motion gradients in MHI converge to the contact point.

D. Robotic Microinjection

In this new robotic system, an operator performs every step throughout the microinjection process via computer mouse clicking. The operator readily selects injection locations (i.e., cell nucleus or cytoplasm) since the cell nucleus and cytoplasm are distinct on a computer monitor. The operator can select a single cell or multiple cells to inject within the field of view. During computer mouse clicking, cell templates centered at the mouse clicking positions are extracted. The templates are used for template matching to provide position feedback. After performing contact detection, the system moves the micropipette tip close to the first target cell and inserts the micropipette into the target cell along the tilting axis at the maximal speed. Injection depth was set to be either 2 μm above the cell bottom surface (i.e., detected by contact on dish substrate) or 2 μm below the cell top surface (i.e., detected by contact on cell membrane). The pressure source is then triggered to apply a positive pressure to deposit the preloaded material into the cell. Material deposition results in a "shock wave" motion inside the cell, around the injection location [see Fig. 5(b)]. The volume of injected materials is precisely controlled by the injection pressure magnitude and width. Although target cells are selected in a random order by the operator, the system injects all cells along the shortest path. The system then moves to the next field of view to continue the injection of more cells. The locations of injected cells are all recorded by the system, permitting time-lapsed imaging of every injected cell.

TABLE I
ROBOTIC MICROINJECTION SPEED OF THREE DIFFERENT CELL LINES

cell line	HeLa	HEK293	HL-1	overall
injection number	2281	1068	1116	4465
injection time (min)	97	48	52	197
speed (cells/min)	23.5	22.3	21.5	22.7

IV. RESULTS AND DISCUSSION

A. Performance of Locating Micropipette Tip

To evaluate the system's performance of automatically locating micropipette, micropipette tip's initial distance to the culture surface was divided into five groups. The task of locating micropipette tips in the five groups was also conducted manually by three skilled micromanipulation operators. Experimental results demonstrate that the overall time for autolocating micropipette tip (30.2 s in an average) is significantly shorter (p-value< 0.001) than in manual operation (averagely 64.8 s). Autolocating micropipette tip was also tested under three imaging modes: bright field, phase contrast, and differential interference contrast (DIC). Although the phase contrast or DIC imaging modes are desired for producing pseudo-3-D view of cells, it was found in experiments that bright field imaging produced a high success rate because the micropipette tip appears more uniform and "halo" free under bight field imaging.

B. Injection Speed

Injection speed of the system was evaluated by injecting three different adherent cell lines: HeLa cells, HEK293 cells, and HL-1 cells. The number of injected cells and time consumed are summarized in Table I. The injection time summarized in Table I is the total experimental time for all steps including locating micropipette tip (after replacement of a new micropipette due to tip damage or clogging), contact detection, cell selection, and injection. The results from the injection of over 4000 cells show that the injection speed of the robotic system is consistent across different adherent cell lines. The average injection speed is 22.7 cells/min, which enables users to inject over a thousand of adherent cells within 1 h.

C. Injection Success Rate and Cell Survival Rate

In order to evaluate the injection success rate and cell survival rate, a Dextran–Rhodamine fluorescent dye was injected into the cytoplasm or nucleus of HeLa cells. The Dextran–Rhodamine dye was chosen because it is highly water soluble and membrane impermeable. Therefore, only the cells that are successfully injected with Dextran–Rhodamine are able to reveal red fluorescent color. The system permits material deposition into the cytoplasm [see Fig. 5(c)] or into the cell nucleus [see Fig. 5(d)]. When the deposition target (i.e., either cytoplasm or nucleus but not both) reveals strong red fluorescent signals, injection was considered successful. Experimental results summarized in Table II show that the success rates for cytoplasmic ($n = 1245$)

TABLE II
INJECTION SUCCESS RATE AND CELL SURVIVAL RATE AFTER INJECTION

injection location	injection number	success rate	survival rate
into cytoplasm	1245	95.2%	97.2%
into nucleus	1036	97.5%	96.5%

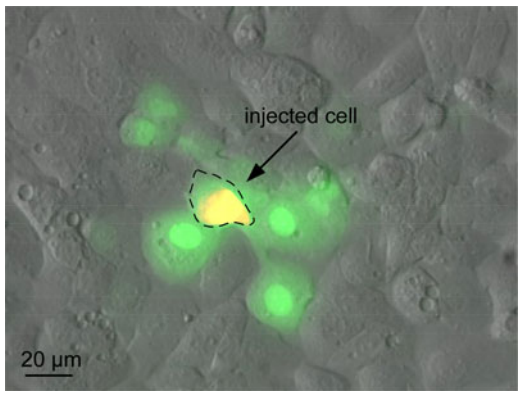

Fig. 6. Only one cell is injected in an area, and fluorescence dye is transferred from the injected cell to adjacent cells through gap junctions.

and nuclear ($n = 1036$) injection were comparable (95.2% and 97.5%).

Cell postinjection viability was evaluated by using a cell viability assay kit (Viability/Cytotoxicity Kit, Life Technologies) after 30 min postinjection incubation. The measured cell survival rate after cytoplasmic injection was 97.2% and after nuclear injection was 96.5%.

D. Characterization of Cell–Cell Communication

We used the robotic system to perform dye transfer experiments for measuring gap junctional intercellular communication (GJIC). In the dye transfer experiments, a membrane-impermeable HPTS (8-Hydroxypyrene-1,3,6-Trisulfonic Acid) fluorescent dye mixing with Dextran–Rhodamine dye was injected into a cell. HPTS fluorescent dye was chosen because of its small molecule size and membrane-impermeable property. The small HPTS molecule (MW = 524.37 Da) can be transferred from the injected cell to adjacent cells through only gap junctions. In contrast, the Dextran–Rhodamine molecule, because of its large molecule size (MW = 10 000 Da), cannot pass through gap junctions. Therefore, only the injected cell reveals a red fluorescent signal, while the injected cell as well as a number of adjacent cells reveal green fluorescent signal (see Fig. 6). The exact number of neighboring cells that can reveal green fluorescent signal is determined by the capability of the cells' gap junctions. Thus, GJIC was quantitatively investigated by measuring the dye transferred cell number (i.e., the number of cells uptaking fluorescent molecules from the injected cell through gap junctions) and dye transferred distance (i.e., the furthest distance that the fluorescent dye can be transferred).

GJIC was investigated on three cell lines (i.e., Hela cells, HEK293 cells, and HL-1 cells). These cell lines are known to have absent, moderate, and high expression of gap junctions, respectively. We also used 18-α glycyrrhetinic acid (18-αGA)

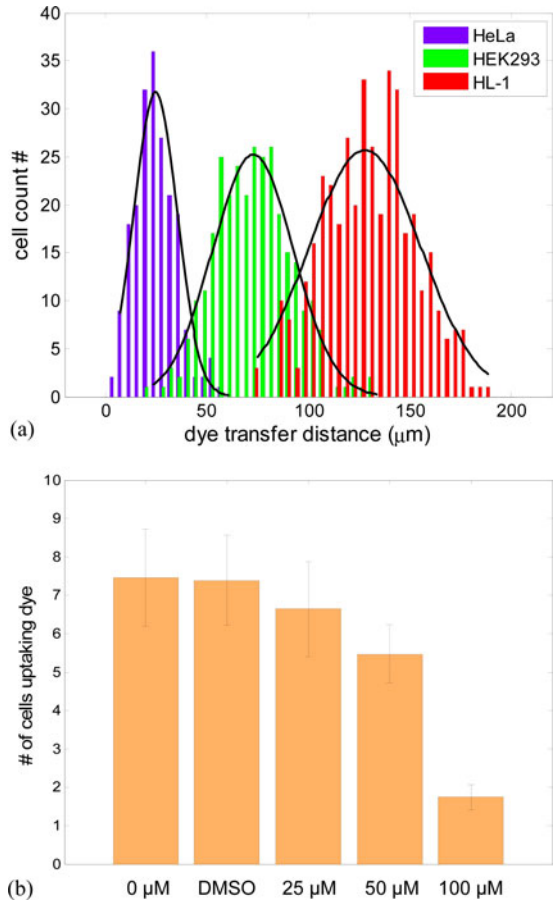

Fig. 7. Results of dye transfer experiments. (a) Histogram of dye transfer distance for HeLa cells ($n = 200$), HEK293 cells ($n = 200$), and HL-1 cells ($n = 400$). (b) Number of HL-1 cells uptaking fluorescence dye from the injected cells. Over 200 cells were injected for each group.

to treat HL-1 cells as a demonstration of quantifying drug effect on regulating gap junction function. It is known that 18-αGA inhibits the role of GJIC in fibroblast growth [22], myoblast fusion [23], and trophoblast proliferation [24]. In our experiments, the robotic system was used to assess GJIC of three experiment groups with different doses (25, 50, or 100 μM) of 18-αGA treatment. Two control groups were also included. Control group 1 [see 0 μM in Fig. 7(b)] had no 18-αGA. Since the 18-αGA stocking solution was dissolved in DMSO, a second control group [see DMSO in Fig. 7(b)] with only DMSO treatment was also examined.

The dye transfer distance was measured to quantitatively characterize the GJIC for the three cell lines. The histogram of dye transfer distance for the three cell lines shown in Fig. 7(a) reveals that HL-1 cells have higher GJIC than the other two cell lines. HL-1 is a cardiac muscle cell line. The strong GJIC of HL-1 cells is physiologically necessary for impulse propagation in cardiac tissue [25]. The impulse signal is passed efficiently through gap junctions, allowing the cardiac tissue to contract at the same tandem. In contrast, Hela cells, a cancer cell line derived from cervical cancer cells, express little GJIC, confirming they do not pass signals via gap junctions for cell coordination. Limited GJIC results in poor inhibition of cancer cell mitosis, causing tumor formation [26].

The experimental data in Fig. 7(b) shows that the number of HL-1 cells that uptook fluorescent dye from the injected cells decreased significantly with a higher dose of GJIC inhibitor. The results show that 100 μM of 18-αGA effectively blocked almost all the gap junctions. There is no significant difference between the two control groups of HL-1 cells [i.e., the first two bars in Fig. 7(b)].

E. Discussion

Microinjection of adherent cells permits the direct insertion of foreign materials (e.g., DNA/RNA, fluorescent dyes, quantum dots, etc.) into single cells. It is a decades-old technology that is still widely used in cell biology for testing cell–cell communication, studying intracellular behavior, and gene transfection [27].

Manual microinjection of adherent cells and existing robotic system prototypes are limited to the injection of a few to tens of cells per experiment at best. Our new robotic system described in this paper is the first system capable of performing microinjection on hundreds and thousands of cells per experiment. The system is embedded with strong automation capabilities in every step of operation, enabling an operator to perform the entire microinjection process via mouse clicking in front of a computer monitor. Training of a user with no skills in microinjection takes 10–15 min, and after a few hours' operation, the user becomes highly proficient at operating the system to perform adherent cell microinjection with high success rates.

V. Conclusion

This paper described a robotic adherent cell injection (RACI) system equipped with several key technologies that were recently developed. These new techniques include automatically locating micropipette tips, robustly detecting the contact of micropipette tip with cell culture surface and directly with cell membrane, and precisely compensating for accumulative positioning errors. The high degree of automation of the system enables users with no microinjection training to perform large-scale cell injection with high success rates. System operation speed, success rate, and cell viability rate were quantitatively evaluated. Dye transfer experiments were conducted on different cell lines to establish a powerful assay for characterizing cell gap junction functions.

References

[1] T. Pawson, "Protein modules and signalling networks," *Nature*, vol. 373, no. 6515, pp. 573–580, Feb. 1995.

[2] P. Friedl and K. Wolf, "Tumour-cell invasion and migration: Diversity and escape mechanisms," *Nat. Rev. Cancer*, vol. 3, no. 5, pp. 362–374, May 2003.

[3] I. Stefanová, J. R. Dorfman, and R. N. Germain, "Self-recognition promotes the foreign antigen sensitivity of naive *T* lymphocytes," *Nature*, vol. 420, no. 6914, pp. 429–434, Nov. 2002.

[4] K. M. Abdullah, G. Luthra, J. J. Bilski, S. A. Abdullah, L. P. Reynolds, D. A. Redmer, and A. T. Grazul-Bilska, "Cell-to-cell communication and expression of gap junctional proteins in human diabetic and nondiabetic skin fibroblasts: Effects of basic fibroblast growth factor," *Endocrine*, vol. 10, no. 1, pp. 35–41, Feb. 1999.

[5] M. Abbaci, M. Barberi-Heyob, W. Blondel, F. Guillemin, and J. Didelon, "Advantages and limitations of commonly used methods to assay the molecular permeability of gap junctional intercellular communication," *BioTechniques*, vol. 45, no. 1, pp. 33–52, Jul. 2008.

[6] Z. Lu, X. Zhang, C. Leung, N. Esfandiari, R. F. Casper, and Y. Sun, "Robotic ICSI (intracytoplasmic sperm injection)," *IEEE Trans. Biomed. Eng.*, vol. 58, no. 7, pp. 2102–2108, Jul. 2011.

[7] H. B. Huang, D. Sun, S. Member, J. K. Mills, and S. H. Cheng, "Robotic cell injection system with position and force control: Toward automatic batch biomanipulation," *IEEE Trans. Robot.*, vol. 25, no. 3, pp. 727–737, Jun. 2009.

[8] A. Pillarisetti, M. Pekarev, A. D. Brooks, and J. P. Desai, "Evaluating the effect of force feedback in cell injection," *IEEE Trans. Autom. Sci. Eng.*, vol. 4, no. 3, pp. 322–331, Jul. 2007.

[9] K. Sakaki, N. Dechev, R. D. Burke, and E. J. Park, "Development of an autonomous biological cell manipulator with single-cell electroporation and visual servoing capabilities," *IEEE Trans. Biomed. Eng.*, vol. 56, no. 8, pp. 2064–2074, Aug. 2009.

[10] Q. Zhao, M. Wu, M. Cui, Y. Qin, J. Yu, M. Sun, X. Zhao, and X. Feng, "A novel pneumatic micropipette aspiration method using a balance pressure model," *Rev. Sci. Instrum.*, vol. 84, no. 12, pp. 123703-1–123703-11, Dec. 2013.

[11] H. Ladjal, J.-L. Hanus, and A. Ferreira, "Micro-to-nano biomechanical modeling for assisted biological cell injection," *IEEE Trans. Biomed. Eng.*, vol. 60, no. 9, pp. 2461–2471, Sep. 2013.

[12] H. Esmaeilsabzali, K. Sakaki, N. Dechev, R. D. Burke, and E. J. Park, "Machine vision-based localization of nucleic and cytoplasmic injection sites on low-contrast adherent cells," *Med. Biol. Eng. Comput.*, vol. 50, no. 1, pp. 11–21, Jan. 2012.

[13] S. Lim, N. A. Zeenathul, M. L. Mohd Azmi, O. Abas Mazni, and O. Fauziah, "Effect of protein concentration and injection pressure in microinjection delivery of maltose binding protein into breast cancer cells," *Pertanika J. Sci. Technol.*, vol. 19, no. 2, pp. 273–283, 2011.

[14] K. Viigipuu and P. Kallio, "Microinjection of living adherent cells by using a semi-automatic microinjection system," *Alternatives Laboratory Animals: ATLA*, vol. 32, no. 4, pp. 417–423, Oct. 2004.

[15] G. Becattini, L. Mattos, and D. Caldwell, "A fully automated system for adherent cells microinjection," *IEEE J. Biomed. Health Informat.*, vol. 18, no. 1, pp. 83–93, Jan. 2014.

[16] W. Wang, Y. Sun, M. Zhang, R. Anderson, L. Langille, and W. Chan, "A system for high-speed microinjection of adherent cells," *Rev. Sci. Instrum.*, vol. 79, no. 10, pp. 104302-1–104302-6, Oct. 2008.

[17] Y. Sun, S. Duthaler, and B. J. Nelson, "Autofocusing in computer microscopy: Selecting the optimal focus algorithm," *Microsc. Res. Tech.*, vol. 65, no. 3, pp. 139–149, Oct. 2004.

[18] J. Liu, Z. Gong, K. Tang, Z. Lu, C. Ru, J. Luo, S. Xie, and Y. Sun, "Locating end-effector tips in robotic micromanipulation," *IEEE Trans. Robot.*, vol. 30, no. 1, pp. 125–130, Feb. 2014.

[19] L. Wang, J. K. Mills, and W. L. Cleghorn, "Automatic microassembly using visual servo control," *IEEE Trans. Electron. Packag. Manuf.*, vol. 31, no. 4, pp. 316–325, Oct. 2008.

[20] W. Wang, X. Liu, and Y. Sun, "Contact detection in microrobotic manipulation," *Int. J. Robot. Res.*, vol. 26, no. 8, pp. 821–828, Aug. 2007.

[21] D. Ziou and F. Deschênes, "Depth from defocus estimation in spatial domain," *Comput. Vis. Image Understanding*, vol. 81, no. 2, pp. 143–165, 2001.

[22] W. Martin, G. Zempel, D. Hülser, and K. Willecke, "Growth inhibition of oncogene-transformed rat fibroblasts by cocultured normal cells: Relevance of metabolic cooperation mediated by gap junctions," *Cancer Res.*, vol. 51, no. 19, pp. 5348–5351, Oct. 1991.

[23] R. M. Mège, D. Goudou, C. Giaume, M. Nicolet, and F. Rieger, "Is intercellular communication via gap junctions required for myoblast fusion?," *Cell Adhesion Commun.*, vol. 2, no. 4, pp. 329–343, Aug. 1994.

[24] T. Nishimura, C. Dunk, Y. Lu, X. Feng, A. Gellhaus, E. Winterhager, J. Rossant, and S. J. Lye, "Gap junctions are required for trophoblast proliferation in early human placental development," *Placenta*, vol. 25, no. 7, pp. 595–607, Aug. 2004.

[25] S. Rohr, "Role of gap junctions in the propagation of the cardiac action potential," *Cardiovascular Res.*, vol. 62, no. 2, pp. 309–322, May 2004.

[26] J. W. Holder, E. Elmore, and J. C. Barrett, "Gap junction function and cancer," *Cancer Res.*, vol. 53, no. 15, pp. 3475–3485, Aug. 1993.

[27] T. K. Kim and J. H. Eberwine, "Mammalian cell transfection: The present and the future," *Anal. Bioanalytical Chem.*, vol. 397, no. 8, pp. 3173–3178, Aug. 2010.

Authors' photographs and biographies not available at the time of publication.